Performance of Simple Timing Synchronization and DC-offset Compensation Schemes for a Short-ranged Bluetooth Network

Young-Hwan You†, Cheol-Hee Park†, Min-Chul Ju†, Jong-Ho Paik†, Jin-Woong Cho†, Hyoung-Kyu Song††

†System IC Research Center, Korea Electronics Technology Institute (KETI), Korea
yhyou@nuri,keti.re.kr
††Department of Information & Communication Engineering, Sejong University, Korea
songhk@sejong.ac.kr

ABSTRACT

This paper describes an adaptive timing synchronization scheme and DC-offset compensation technique for a short-ranged Bluetooth system. The synchronization scheme estimates the variance of the partial-band interference, which is utilized for the trigger threshold value of the inquiry scan and page scan states, while DC-offset compensation scheme is designed using the access codes which are known to each Bluetooth device. Numerical results show the proposed synchronization algorithm is robust to the partial-band noise interference and of low complexity. Also, the new DC-offset compensation method shows more reliable estimation ability of DC-offset than the existing method without extra hardware burdens.

1. INTRODUCTION

Recently, much attention have been brought to a new class of home- and personal-area network (PAN) devices. Utilizing low-cost technologies like HomeRF, HomeCast, and Bluetooth, they will use wireless links to both access wide-area communications and exchange data amongst themselves [1][2]. Especially, Bluetooth is focused on a low-cost short-range radio link, facilitating protected ad-hoc connections for stationary and mobile communication environments [1].

Bluetooth transceiver operates in the unlicensed 2.4 GHz ISM band. Cordless phones, garage door opener, microwave ovens, and other PAN devices such as HomeRF and IEEE 802.11 operate in this band, where microwave ovens are the strongest source of interference. In the Bluetooth system, using a frequency-hop technique and error correction algorithms, the interference protection can be achieved [1]. However, the interferences from other PAN devices operated in the ISM band will prevent Bluetooth units from establishing reliable synchronizations and connections.

This paper is concerned with an adaptive timing synchronization scheme and DC-offset compensation scheme in the frequency-hopped Bluetooth system. First, the performance of the synchronization receiver is examined in the presence of the partial-band noise jamming in terms of the detection probability. The proposed timing synchronization technique is robust to the partial-band noise interference and has a good estimation accuracy with a low complexity. Second, the DC-offset compensation scheme is designed using a trigger value of the pre-sliding correlator to indicate a start of DC-offset compensation instead of using a short preamble and trailer of access code. The new DC-offset compensation method shows more reliable estimation ability of DC-offset than the existing method. Also, this algorithm can be implemented without degradation of frame and spectral efficiency thanks to using the access code specified for Bluetooth system.

0-7803-6465-5/00 $10.00 © 2000 IEEE

2. BLUETOOTH SYSTEM AND CHANNEL MODEL

2.1 Bluetooth overview

The connect procedure is initiated by one of the unit, the master, which should know the address and clock register value of the other units for the connection. A connection is made either by a page message if the address is already known and clock register value is unknown, or by the inquiry message followed by a subsequent page message if both of the address and clock register value are unknown. When a node receives a packet, it checks the packet identification, and if it is not the destination, transits the next state. There are two major states: standby and connection; in addition, there are seven substates denoted as page, page scan, inquiry, inquiry scan, master response, slave response, and inquiry response. In the connection state, the Bluetooth units can be several low-power modes; active mode, sniff mode, hold mode, and park mode. In this paper, the inquiry and inquiry scan states are denoted as the initial state.

2.2 Channel model

A binary GFSK with modulation index between 0.28 and 0.35 is employed for a simple and small transceiver implementation. A transmitted GFSK signal can be written as

$$p(t) = \mathrm{Re}\left\{\sqrt{\frac{2E}{T}}e^{j2\pi\{f_c t + h\int_{-\infty}^{t} g(\tau)d\tau\}}\right\} \quad (1)$$

where E is the energy per symbol, T is the symbol period, f_c is the carrier frequency, h is the modulation index, and $g(t)$ is the output of Gaussian low pass filter (GLPF) for a NRZ data signal. The output of GLPF can be expressed as

$$g(t) = \sum_{k=-\infty}^{\infty} a_k v(t - kT) \quad (2)$$

where $a_k = \pm 1$ and

$$v(t) = \frac{1}{2}\{\mathrm{erf}(-\lambda B_b T) + \mathrm{erf}(\lambda B_b(t+T))\} \quad (3)$$

In eqn. (3), $\lambda = \sqrt{2/\ln 2}\pi$, $B_b T = 0.5$, B_b is a 3 dB bandwidth of GLPF, and $\mathrm{erf}(t) = \int_0^t \frac{2}{\sqrt{\pi}} e^{-t^2} dt$.

We use a statistical channel model for the indoor radio propagation. The low-pass equivalent channel impulse response is given by [3]

$$c(t) = \sum_{l=0}^{\infty}\sum_{k=0}^{\infty} \gamma_{kl} e^{j\theta_{kl}} \delta(t - T_l - \tau_{kl}) \quad (4)$$

where T_l is the arrival of the l-st cluster, τ_{kl} is the arrival time of the k-th ray measured from the beginning of the l-st cluster, θ_{kl} is the phase shift, and γ_{kl} is the power gain of the k-th ray in the 1-st cluster. We assume that the Bluetooth system operates in the indoor environment with a rms delay spread of 50 ns, a maximum delay spread of 300 ns, and Doppler spread of 10 Hz [3]. The modulated GFSK signal is transmitted at a 1 Mbit/s rate in 625 μs slot size, which makes the assumption that the channel is fixed within a slot.

The received GFSK signal $s(t)$ can be written by

$$\begin{aligned} s(t) &= m(t)c(t) + n(t) \\ &= \sqrt{\frac{2E}{T}} C(t) e^{j(\phi(t,\bar{a}) + \phi_c(t))} + N(t) e^{j\phi_n(t)} \end{aligned} \quad (5)$$

where $c(t) = C(t)e^{j\phi_c(t)}$ is the component of the channel distortion, $n(t) = N(t)e^{j\phi_n(t)}$ is the additive white Gaussian noise (AWGN), and $m(t) = \sqrt{2E/T}e^{j\phi(t,\bar{a})}$ is equivalent complex envelope of $p(t)$.

3. ADAPTIVE TIMING SYNCHRONIZATION SCHEME IN BLUETOOTH SYSTEMS

3.1 Adaptive timing synchronization in the initial state

A block diagram of the FH/GFSK receiver with an adaptive synchronization is shown in Fig. 1. The receiver consists of two channels; one tuned to baseband frequency f_1 corresponding to "space" and the other to frequency f_2 corresponding to "mark". After down-converting and dehopping by the frequency synthesizer, the dehopped signal is then to be processed by the square-law combining FSK receiver [4]. The detector outputs are sampled once every bit duration and the difference between the outputs of two channels is correlated with the inquiry access code (IAC) or device access code (DAC) to produce correlation output Z_f. The estimated noise variance is multiplied by weighting factor K_1 to produce a synchronization threshold $\sigma_k^2 K_1$. If the correlation output exceeds $\sigma_k^2 K_1$, the Bluetooth unit will transit inquiry response state, responding a frequency hop synchronization (FHS) packet, when it is in the inquiry scan state and enter slave response substate, replying DAC, when in the page scan state [1].

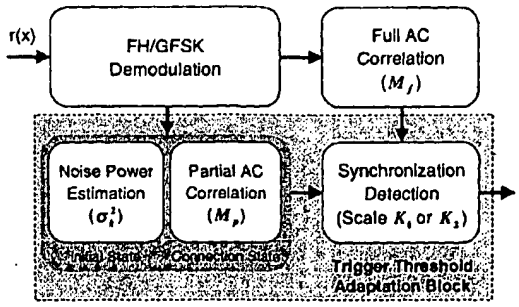

Fig. 1. An adaptive synchronization receiver in Bluetooth systems

In practice, the measurement of noise power cannot be accomplished perfectly. As described in [5], however, using reciprocal of the sum of the outputs of the two quadratic detectors achieves the same noise-limited improvement effect as the above mentioned receiver whose performance is based on the perfect estimation of noise power. For analysis purposes, therefore, we have assumed that the measurement of noise variance produces σ_k^2 exactly and the pulse response of a Gaussian LPF is rectangular.

3.2 Detection probability in the initial state

The region of time/frequency uncertainty of the transmitted phase is divided into samples with one of them denoting the sync-sample (Hypothesis H_1) and the others the nonsync-samples (Hypothesis H_0). According to the transmitted signal ("space" and "mark"), the sampled detector output of each channel can be represented as

$$r_k^{(s/m)} = \begin{cases} \left(\Lambda_{\cos}^{(s/m),1k}\right)^2 + \left(\Lambda_{\sin}^{(s/m),2k}\right)^2, & \text{if energy detected} \\ n_{3k}^{(s/m)^2} + n_{4k}^{(s/m)^2}, & \text{if energy not detected} \end{cases} \quad (6)$$

where $\Lambda_{\cos/\sin}^{(s/m),\,ik} = \sqrt{2P}\cos/\sin\theta_k^{(s/m)} + n_{ik}^{(s/m)}$, P is the signal power, $\{\theta_k^{(s/m)}\}$ are the uniform phase random variable, $\{n_{ik}^{(s/m)}\}$ are the independent zero-mean Gaussian with variance σ_k^2 in each channel, and (s/m) notation denotes the corresponding term-wise pair.

Under the assumption of the same average noise power in both "mark" and "space" channels, after correlating the difference between the outputs of two channels with IAC or DAC, the output of the correlator of H_1 sample is expressed as

$$Z_f = \frac{1}{M_f}\left\{\sum_{k=1}^{M_f^{+1}} \sigma_k^2\left[\left(\Omega_{\cos}^{(s),1k}\right)^2 + \left(\Omega_{\sin}^{(s),2k}\right)^2 - \omega_k^{(s)^2}\right] + \sum_{k=1}^{M_f^{-1}} \sigma_k^2\left[\left(\Omega_{\cos}^{(m),1k}\right)^2 + \left(\Omega_{\sin}^{(m),2k}\right)^2 - \omega_k^{(m)^2}\right]\right\} \tag{7}$$

where $\Omega_{\cos/\sin}^{(x),\,ik} = \sqrt{\frac{2P}{\sigma_k^2}}\cos/\sin\theta_k^{(x)} + w_{ik}^{(x)}$, $\omega_k^{(x)^2} = w_{3k}^{(x)^2} + w_{4k}^{(x)^2}$, $M_f = M_f^{+1} + M_f^{-1}$, $\{w_{ik}^{(s/m)}\}$ are independent Gaussian random variables with zero mean and unit variance, and the received noise power of each channel is $\sigma_k^2 = N_0B$ with probability $1-r$ and $\sigma_k^2 = (N_0 + N_J/r)B$ with probability r, respectively. M_f^{+1} is the number of one's in the access code, M_f^{-1} is the number of zero's in the access code, B is the cell bandwidth, and N_0 and N_J are the thermal noise spectral density and the average jamming noise spectral density, respectively.

To evaluate the probability distribution function (PDF) of correlation output, based on the central limit theorem, we have assumed that the correlation term is Gaussian. Fortunately, since a 64-bit synchronization word is used in the Bluetooth system (i.e., $M_f = 64$), such an approximation is certainly feasible. From the above discussions, the PDF of Z_f under hypothesis H_1, $p_f(z|H_1)$, follows the Gaussian distribution with mean $m_f = 2P$ and variance $\sigma_f^2 = 8(\sigma_k^2 P + \sigma_k^4)/M_f$.

Under the assumption that the noise power is estimated exactly, the detection probability, P_D, is the probability that the H_1 sample exceeds the threshold $\sigma_k^2 K_1$, which can be evaluated as

$$P_D = (1-r)Q\left(\frac{K_1 - 2\rho_1}{\zeta_1}\right) + rQ\left(\frac{K_1 - 2\rho_2}{\zeta_2}\right) \tag{8}$$

where $\rho_1 = E_b/N_0$, $\rho_2 = E_b/(N_0 + N_J/r)$, $\zeta_i = \sqrt{8(\rho_i+1)/M_f}$, and $Q(x) = \int_x^\infty \frac{1}{\sqrt{2\pi}} e^{-\frac{t^2}{2}}\,dt$.

3.3 Numerical results and discussions

Numerical behaviors of the proposed synchronization scheme in the Bluetooth network are presented in this section. Throughout this section the parameters $M_f = 64$ and $B = 1$ MHz are assumed. The values of weighting factor K_1 is chosen to ensure P_{FA} an acceptable rate for each value of E_b/N_0 and E_b/N_J.

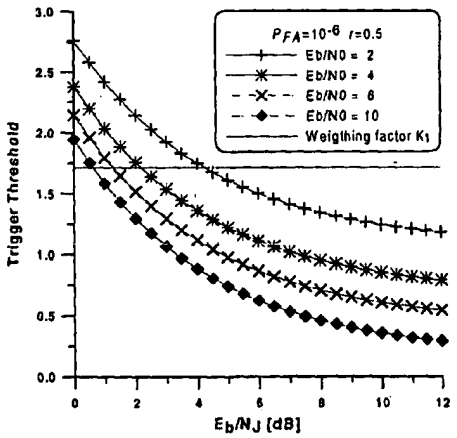

Fig. 2. Trigger threshold versus E_b/N_J for various values of E_b/N_0 ($P_{FA} = 10^{-6}$ and $r = 0.5$)

Figs. 2 ~ 3 present the performance of the timing synchronization receiver in the initial state for various system and channel parameters under the partial-band noise environments. Though the master does not broadcast message, the correlation output of slave's unit may exceed the threshold $\sigma_k^2 K_1$ due to the noise interferences during the initial state. Under hypothesis H_0, this happens with probability $P_{FA} = (1-r)Q(K_1/\zeta_1) + rQ(K_1/\zeta_2)$.

Fig. 2 presents the actual trigger threshold versus E_b/N_J with $r = 0.5$ and $P_{FA} = 10^{-6}$. The solid line represents the values of K_1 for various values of E_b/N_0 and E_b/N_J. It is clear from Fig. 2 that values of the weighting factor K_1 is insensitive to the partial-band noise interferences and an adaptive setting of the actual trigger threshold can be obtained by setting the weighting factor to a fixed value.

Performance of the synchronization receiver for various values of partial-band jamming fractions r and E_b/N_0 with $P_{FA} = 10^{-6}$ is shown in Fig. 3. As expected, for lower E_b/N_J, a severe degradation in the detection probability due to the partial-band jamming noise is observed. For a partial-band jamming fraction of $r = 1$, however, the performance degradation according to the variation of E_b/N_0 is negligible, which is thanks to the deemphasis of jammed hops provided by the nonlinear combining scheme.

4. DC-OFFSET ESTIMATOR FOR BLUETOOTH SYSTEM

4.1 Analog DC-offset estimator

Fig. 4 depicts the structure of the proposed DC-offset estimator. The function of the pre-sliding correlator is same

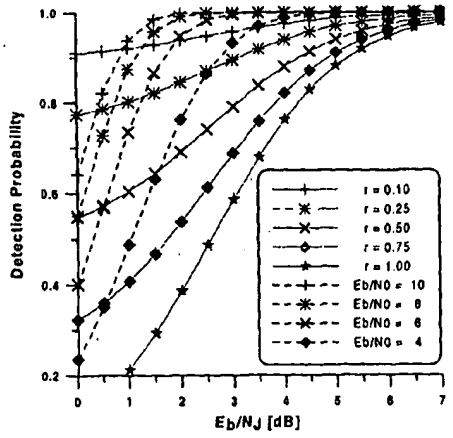

Fig. 3. Performance of the synchronization receiver for various values of r and E_b/N_0 with $P_{FA} = 10^{-6}$: (1) solid line - $E_b/N_0 = 2$ [dB] and (2) dashed line - $r = 1.0$

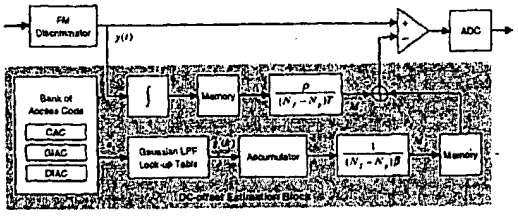

Fig. 4. The structure of the proposed DC-offset compensator

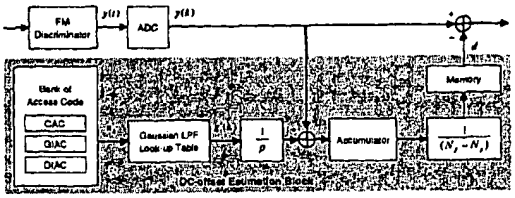

Fig. 5. The structure of the digital DC-offset compensator using LS method

to that of the pre-sliding correlator used in the channel estimator of the previous section. As described in Section 4, a trigger event activates the DC-offset estimation. At the receiver, the output of the GLPF for the access code detected by the pre-sliding correlator (i.e., the replica for the transmitted access code) is regenerated, which is utilized as the reference signal. Comparing the received signal with the regenerated signal and adopting a simple LS algorithm, the DC-offset estimation is performed. After receiving the access code, if the active member address (AMA) of the packet header is synchronized to its own AMA, the slave works on and the estimated value for the channel distortion is used during one slot (625 μs); otherwise, the receiver goes to sleep until the next RX event.

Using the known access code, the regenerated output of GLPF for the access code a'_k can be expressed as

$$g'(t) = \sum_{k=0}^{N_f-1} a'_k v(t - kT) \tag{9}$$

The regenerated signal for the access code selected by a pre-sliding correlator can be implemented with a look-up table and the signal is over-sampled at the rate of β/T. Thus, the stored samples in the look-up table can be represented by

$$g'(n) = \sum_{k=0}^{N_f-1} a'_k v(nT/\beta - kT),\ n = 0, 1, \cdot, \beta N_f - 1 \tag{10}$$

Using the look-up table, the regenerated signals of the selected access code are accumulated and averaged over $(N_f - N_p)\beta$ samples, which is used for a reference value of the DC-offset estimation and can be expressed as

$$M_s = \frac{1}{(N_f - N_p)\beta} \sum_{n=\beta N_p}^{\beta N_f - 1} \sum_{k=0}^{N_f-1} a'_k v(nT/\beta - kT) \tag{11}$$

On the other hand, in Fig. 4, the output of the FM discriminator is integrated and averaged within the time interval $(N_f - N_p)T$, which results in

$$M_r = \frac{\rho}{(N_f - N_p)T} \int_{N_p T}^{(N_f-1)T} y(t)dt \tag{12}$$

where $\rho = 1/(\pi h)$ is the normalized factor. Using eqn. (11) and (12), finally, the estimated DC-offset can be obtained as $d = M_s - M_r$.

4.2 Digital DC-offset estimator

As a comment of the implementation of the proposed DC-offset estimator, it is efficiently designed into a digital circuit. In this digital-stage DC-offset estimator, the regenerated reference signal $g'(k)$ can be expressed in an identical form to eqn. (10) with $\beta = 1$ and be also written in terms of the sampled output $y(k)$ as follows

$$g'(k) = \rho\{y(k) - d - e(k)\} \tag{13}$$

where $e(k)$ is error term due to the imperfect compensation.

The performance index $I(d)$ is the euclidean norm of the error vector e, which is given by

$$I(d) = (\mathbf{y} - \mathbf{g}'/\rho - \mathbf{d})^T(\mathbf{y} - \mathbf{g}'/\rho - \mathbf{d}) \tag{14}$$

where $\mathbf{g}'$ is the vector of regenerated GLPF outputs for the access code and $\mathbf{d}$ is the vector of the estimated DC-offset. The LS optimization involves the minimization of

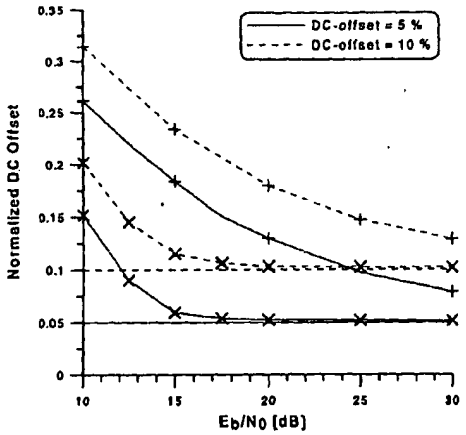

Fig. 6. The estimation ability of DC-offset for both the conventional and proposed DC-offset estimator with DC-offset 5 % and 10 % : (1) + - the existing method, (2) × - the proposed method, (3) None - DC offset value

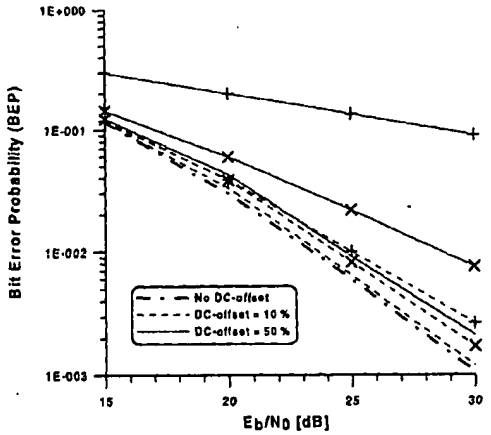

Fig. 7. The BEP performance of the DC-offset compensators with DC-offset 10 % and 50 % : (1) + - no DC-offset compensation, (2) × - the conventional DC-offset compensation, (3) None - the proposed DC-offset compensation

$I(d)$ and the value of d which minimizes $I(d)$ is given by

$$d = \frac{1}{N_f - N_p}\left(\sum_{k=N_p}^{N_f-1} y(k) - \frac{1}{\rho}\sum_{k=N_p}^{N_f-1} g'(k)\right) \quad (15)$$

Referring to eqn. (18), the proposed DC-offset estimator is implemented at the digital stage as shown in Fig. 5. It is note that the scale factor ρ can be varied on the condition of the channel and receiver. Therefore, this value is calculated by solving the equation $\frac{\partial I}{\partial(1/\rho)} = 0$, which gives a solution $\rho = \mathbf{g'}^T\mathbf{g'}/(\mathbf{y}^T\mathbf{g'} - \mathbf{g'}^T\mathbf{d})$. Finally, the value of d which minimizes $I(d)$ can be rewritten as

$$d = \frac{\mathbf{g'}^T\mathbf{g'}\sum_{k=N_p}^{N_f-1} y(k) - \mathbf{y}^T\mathbf{g'}\sum_{k=N_p}^{N_f-1} g'(k)}{(N_f - N_p)\mathbf{g'}^T\mathbf{g'} - \left\{\sum_{k=N_p}^{N_f-1} g'(k)\right\}^2} \quad (16)$$

4.3 Simulation results and discussions

Throughout this section the parameters $N_f = 72$, $N_p = 10$, $B_bT = 0.5$, and $B = 1$ MHz are assumed. Also, a binary GFSK with modulation index 0.3 is employed.

The estimation ability of DC-offset for both the conventional and proposed DC-offset estimator is presented in Fig. 6. We see from Fig. 6 that the proposed DC-offset estimator tracks more accurately the DC-offset values for a large range of E_b/N_0 than the conventional one.

Fig. 7 shows the BEP performance with DC-offset values in the input signal of 10 % and 50 % of the ADC half scale. The BEP performance with the DC-offset estimator, without DC-offset estimator, of no DC-offset is also shown in the figure. In the case of 50 % DC-offset, the E_b/N_0 degradation from the ideal at a BEP of 10^{-2} is 5.5 dB for the conventional method and 1.5 dB for the proposed method. For the case of DC-offset 10 %, on the other hand, the required E_b/N_0 at a BEP of 10^{-2} is degraded by 0.8 dB for the conventional scheme and 1.8 dB for the proposed scheme compared to the E_b/N_0 without using DC-offset estimator, and further improvement can be obtained for a large value of DC-offset.

5. CONCLUSIONS

The performance of the proposed synchronization receivers for a short-ranged radio system has been addressed. The synchronization performance is robust against the partial-band noise jamming interferences. Furthermore, the DC-offset estimation scheme is very effective for solving the problem of the channel distortion for the implementation of the existing Bluetooth system without degradation of frame and spectral efficiency, whic is thanks to using the access code specified for the Bluetooth system. Especially, these schemes is suitable for the low-cost and low-complexity technologies like Bluetooth, HomeRF, and HomeCast.

REFERENCES

[1] Bluetooth SIG groups, "Specification of the bluetooth system," ver 1.0 draft foundation, July 1999.
[2] HomeRF, "Technical summary of the SWAP specification," February 1999.
[3] K. Pahlavan and A. H. Levesque, *Wireless information networks*, Wiley-Interscience Publication, 1995.
[4] J. S. Lee, R. H. French, and L. E. Miller, "Probability of error analyses of a BFSK frequency-hopping system with diversity under partial-band jamming interference-Part I: Performance of a square-law linear combining soft decision receiver," *IEEE Trans. Commun.*, vol. 32, no. 6, pp. 645-653, June 1984.
[5] L. E. Miller, J. S. Lee, and A. P. Kadrichu, "Probability of error analyses of a BFSK frequency-hopping system with diversity under partial-band jamming interference-Part III: Performance of a square-law self-normalizing soft decision receiver," *IEEE Trans. Commun.*, vol. 34, no. 7, pp. 669-675, July 1986.
[6] F. Bennet *et al.*, "Piconet: embedded mobile networking," *IEEE Personal Commun.*, pp. 8-15, October 1997.
[7] J. G. Proakis, *Digital Communications*, 2nd Ed. New York: MacGraw-Hill, 1989.

ADAPTIVE TIMING SYNCHRONIZATION SCHEMES FOR A SHORT-RANGED BLUETOOTH SYSTEM

Young-Hwan You[1], Min-Chul Ju[1], Jong-Ho Paik[1], Jin-Woong Cho[1] and Hyoung-Kyu Song[2]
[1]System IC Research Center, Korea Electronics Technology Institute (KETI), Korea
[2]Department of Information & Communication Engineering, Sejong University, Korea

ABSTRACT

This paper describes two adaptive timing synchronization schemes for a short-ranged Bluetooth system in the partial-band noise environments. One estimates the variance of the partial-band interference, which is utilized for the trigger threshold value of the inquiry scan and page scan states, while second is designed using the scaled partial correlation value for the connection state. Numerical results show the proposed synchronization algorithms are robust to the partial-band noise interference and of low complexity, which is suitable for a low-cost personal area network (PAN).

1. INTRODUCTION

Recently, much attention have been brought to a new class of home- and personal-area network (PAN) devices with low-cost technologies such as HomeRF, HomeCast, and Bluetooth [1][2]. Especially, Bluetooth is focused on a low-cost short-range radio link, facilitating protected ad-hoc connections for stationary and mobile communication environments as shown in Fig. 1.

Bluetooth transceiver operates in the unlicensed 2.4 GHz ISM band. Cordless phones, garage door opener, microwave ovens, and other PAN devices such as HomeRF and IEEE 802.11 also operate in this band and among these devices microwave ovens are the strongest source of interference. In the Bluetooth system, using a frequency-hop (FH) technique and error correction algorithms, the interference protection can be achieved [1]. However, the interferences from other PAN devices operated in the ISM band will prevent Bluetooth units from establishing reliable synchronizations and connections.

This paper is concerned with two adaptive timing synchronization schemes in the frequency-hopped Bluetooth system. The performance of the synchronization receivers is examined in the presence of the partial-band noise jamming in terms of the detection probability. In this paper, we consider the partial-band interference, which may be due to a partial-band jammer as well as other unwanted narrowband interferences, and is modeled as additive Gaussian noise [3][4]. Furthermore, the interference is assumed to be present in a frequency shift keying (FSK) demodulator for any reception of the dehopped signal with probability r. The proposed timing synchronization techniques are robust to the partial-band noise interference and have a good estimation accuracy with a low complexity.

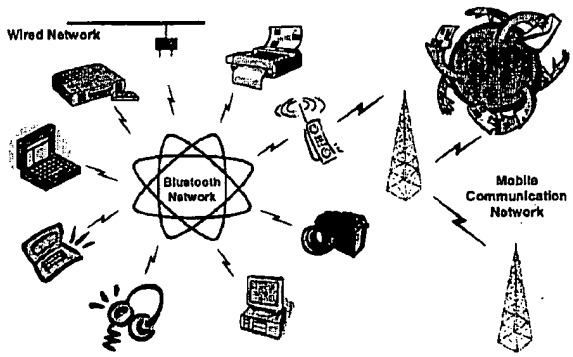

Fig. 1. Bluetooth network

The outline of the paper is organized as follows. Section 2 describes the Bluetooth system model and the connection process. In Section 3 and 4, the proposed timing synchronization algorithms and their performance are presented in detail, respectively. Some numerical results are presented in Section 5. Finally, the concluding remarks are given in Section 6.

2. BLUETOOTH SYSTEM

2.1 Overview of Bluetooth system

Bluetooth uses a slotted time-division duplex (TDD) scheme for full-duplex transmission, where each slot is 0.625 ms long (two slots form one frame) and a Gaussian-shaped FSK (GFSK) modulation is applied to minimize transceiver com-

Original manuscript received June 19, 2000

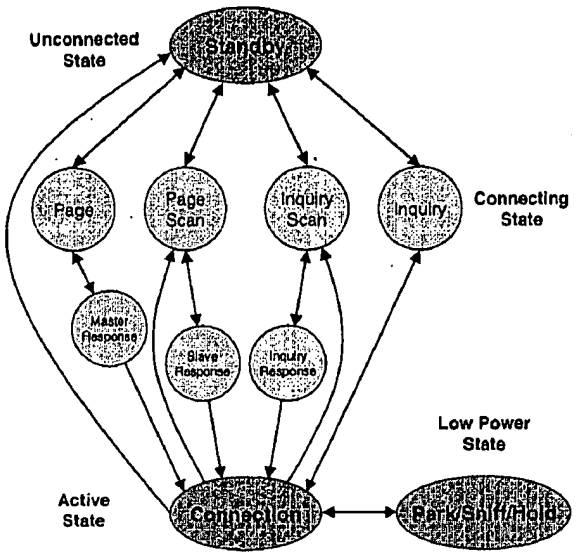

Fig. 2. State diagram of Bluetooth link controller

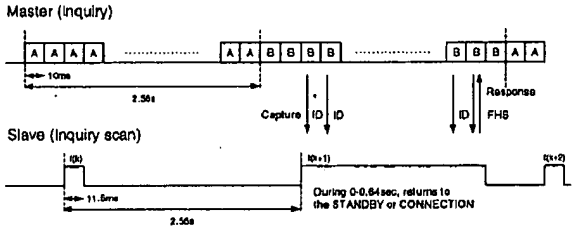

Fig. 3. Inquiry and inquiry scan states in Bluetooth systems [1]

plexity. The Bluetooth radio uses a fast frequency hopping scheme and short data packets to make the link robust in a noisy radio environment. In addition, the use of forward error correction (FEC) limits the impact of random noise. The physical communication range will be in the interval 10 cm to 10 m, but can be extended to above 100 m, which is controlled by the transceiver power in the range -30 dBm to 20 dBm with a nominal value of 0 dBm.

The Bluetooth baseband protocol is a combination of circuit switching and packet switching, where time slots can be reserved for packets carrying synchronous information (synchronous connection oriented voice link) or dynamically allocated for asynchronous information (asynchronous connectionless data link).

2.2 Connection procedure of Bluetooth units

In the ad-hoc network, several mobile nodes (e.g., notebook computer, printer, mobile phone, and headset) may get together in a small area and establish peer-to-peer communication among themselves without the help of any infrastructure such as a wired/wireless backbone. When first establishing a network or adding components to a piconet, the units must be identified. Units can be dynamically connected and disconnected from the piconet at any time [5].

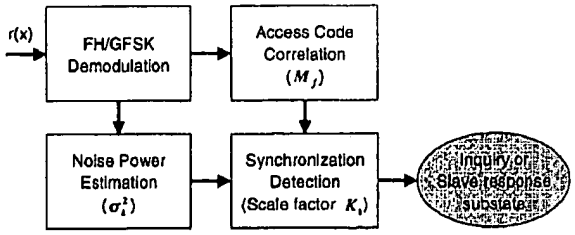

Fig. 4. An adaptive synchronization receiver in the initial state

The connect procedure is initiated by one of the unit, the master, which should know the address and clock register value of the other units for the connection. A connection is made either by a page message if the address is already known and clock register value is unknown, or by the inquiry message followed by a subsequent page message if both of the address and clock register value are unknown. When a node receives a packet, it checks the packet identification, and if it is not the destination, transits the next state. Fig. 2 describes a state diagram illustrating the states used in the Bluetooth link controller. As shown in Fig. 2, there are two major states: standby and connection; in addition, there are seven substates denoted as page, page scan, inquiry, inquiry scan, master response, slave response, and inquiry response. In the connection state, the Bluetooth units can be several low-power modes; active mode, sniff mode, hold mode, and park mode. The functional description of inquiry and inquiry scan procedures is summarized in Fig. 3. The page and page scan substates are similar to the inquiry and inquiry scan procedures, respectively [1]. In this paper, the inquiry and inquiry scan states are denoted as the initial state.

3. ADAPTIVE TIMING SYNCHRONIZATION SCHEMES IN BLUETOOTH SYSTEMS

3.1 Adaptive timing synchronization in the initial state

A block diagram of the FH/GFSK receiver with an adaptive synchronization is shown in Fig. 4. The receiver consists of two channels; one tuned to baseband frequency f_1 corresponding to "space" and the other to frequency f_2 corresponding to "mark". After down-converting and dehopping by the frequency synthesizer, the dehopped signal is then to be processed by the square-law combining FSK receiver [3]. The detector outputs are sampled once every bit duration and the difference between the outputs of two channels is cor-

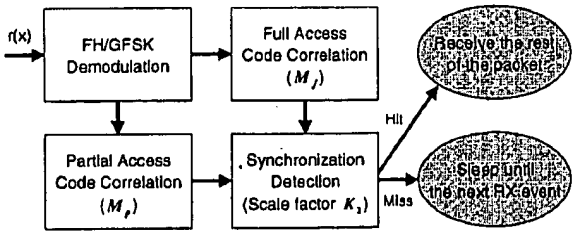

Fig. 5. An adaptive synchronization receiver in the connection state

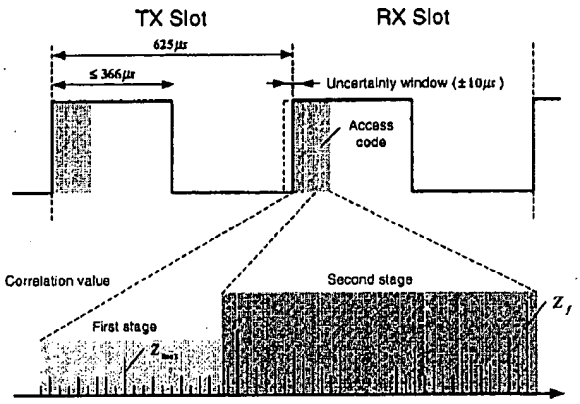

Fig. 6. An example of the correlation outputs in normal mode of the connection state with no timing slipping

related with the inquiry access code (IAC) or device access code (DAC) to produce correlation output Z_f. The estimated noise variance is multiplied by weighting factor K_1 to produce a synchronization threshold $\sigma_k^2 K_1$. If the correlation output exceeds $\sigma_k^2 K_1$, the Bluetooth unit will transit inquiry response state, responding a frequency hop synchronization (FHS) packet, when it is in the inquiry scan state and enter slave response substate, replying DAC, when in the page scan state [1].

In practice, the measurement of noise power cannot be accomplished perfectly. As described in [4], however, using reciprocal of the sum of the outputs of the two quadratic detectors achieves the same noise-limited improvement effect as the above mentioned receiver whose performance is based on the perfect estimation of noise power. For analysis purposes, therefore, we have assumed that the measurement of noise variance produces σ_k^2 exactly and the pulse response of a Gaussian LPF is rectangular.

3.2 Adaptive timing synchronization in the connection state

In the connection state, the connection has been established and packets can be sent back and forth. In both master and slave units, the channel access code and the master Bluetooth clock are used. During the beginning of the RX cycle, as shown in Fig. 5, the pre-sliding access correlator with length of $M_p < M_f$ searches for the correct access code over the uncertainty region with length of 20 μs. After $(20 + M_p)$ μs, therefore, $N_w = 20$ partial correlation values are collected and the largest of the resulting N_w outputs of a pre-sliding correlator, Z_{max}, is chosen, which is multiplied by scale factor K_2. The corresponding phase of the largest value is assumed, tentatively, to be coarsely aligned with the received access code signal. After correlating with the remaining $(M_f - M_p)$-bit access code, finally, the full correlation value for access code is produced and compared with $K_2 Z_{max}$. If a trigger event does occur, the receiver remains open to receive the rest of the packet, which happens with probability P_D if it is actually the correct phase; otherwise, the receiver goes to sleep until the next RX event. Fig. 6 gives an example for the operation of access code searcher in the case of no timing slipping.

4. DETECTION PERFORMANCE OF THE SYNCHRONIZATION RECEIVER

In deriving the probability expressions, we assume that the correlation of the specular sequence and the local access code is negligibly small and can be ignored when they are out of phase (H_0 samples).

4.1 Detection probability in the initial state

The region of time/frequency uncertainty of the transmitted phase is divided into samples with one of them denoting the sync-sample (Hypothesis H_1) and the others the nonsync-samples (Hypothesis H_0). According to the transmitted signal ("space" and "mark"), the sampled detector output of each channel can be represented as

$$r_k^{(s/m)} = \begin{cases} \left(\Lambda_{\cos}^{(s/m),\,1k}\right)^2 + \left(\Lambda_{\sin}^{(s/m),\,2k}\right)^2, & \text{if energy detected} \\ n_{3k}^{(s/m)^2} + n_{4k}^{(s/m)^2}, & \text{if energy not detected} \end{cases} \quad (1)$$

where $\Lambda_{\cos/\sin}^{(s/m),\,ik} = \sqrt{2P}\cos/\sin\theta_k^{(s/m)} + n_{ik}^{(s/m)}$, P is the signal power, $\{\theta_k^{(s/m)}\}$ are the uniform phase random variable, $\{n_{ik}^{(s/m)}\}$ are the independent zero-mean Gaussian with variance σ_k^2 in each channel, and (s/m) notation denotes the corresponding term-wise pair.

Under the assumption of the same average noise power in both "mark" and "space" channels, after correlating the difference between the outputs of two channels with IAC or DAC, the output of the correlator of H_1 sample is expressed

as

$$Z_f = \frac{1}{M_f}\left\{\sum_{k=1}^{M_f^{+1}} \sigma_k^2\left[\left(\Omega_{\cos}^{(s),\,1k}\right)^2 + \left(\Omega_{\sin}^{(s),\,2k}\right)^2 - \omega_k^{(s)^2}\right] + \sum_{k=1}^{M_f^{-1}} \sigma_k^2\left[\left(\Omega_{\cos}^{(m),\,1k}\right)^2 + \left(\Omega_{\sin}^{(m),\,2k}\right)^2 - \omega_k^{(m)^2}\right]\right\} \tag{2}$$

where $\Omega_{\cos/\sin}^{(x),\,ik} = \sqrt{\frac{2P}{\sigma_k^2}}\cos/\sin\theta_k^{(x)} + w_{ik}^{(x)}$, $\omega_k^{(x)^2} = w_{3k}^{(x)^2} + w_{4k}^{(x)^2}$, $M_f = M_f^{+1} + M_f^{-1}$, $\{w_{ik}^{(s/m)}\}$ are independent Gaussian random variables with zero mean and unit variance, and the received noise power of each channel is $\sigma_k^2 = N_0B$ with probability $1-r$ and $\sigma_k^2 = (N_0 + N_J/r)B$ with probability r, respectively. M_f^{+1} is the number of one's in the access code, M_f^{-1} is the number of zero's in the access code, B is the cell bandwidth, and N_0 and N_J are the thermal noise spectral density and the average jamming noise spectral density, respectively.

To evaluate the probability distribution function (PDF) of correlation output, based on the central limit theorem, we have assumed that the correlation term is Gaussian [6]. Fortunately, since a 64-bit synchronization word is used in the Bluetooth system (i.e., $M_f = 64$), such an approximation is certainly feasible. From the above discussions, the PDF of Z_f under hypothesis H_1, $p_f(z|H_1)$, follows the Gaussian distribution with mean $m_f = 2P$ and variance $\sigma_f^2 = 8(\sigma_k^2P + \sigma_k^4)/M_f$.

Under the assumption that the noise power is estimated exactly, the detection probability, P_D, is the probability that the H_1 sample exceeds the threshold $\sigma_k^2K_1$, which can be evaluated as

$$P_D = (1-r)Q\left(\frac{K_1 - 2\rho_1}{\zeta_1}\right) + rQ\left(\frac{K_1 - 2\rho_2}{\zeta_2}\right) \tag{3}$$

where $\rho_1 = E_b/N_0$, $\rho_2 = E_b/(N_0 + N_J/r)$, $\zeta_i = \sqrt{8(\rho_i+1)/M_f}$, and $Q(x) = \int_x^\infty \frac{1}{\sqrt{2\pi}}e^{-\frac{t^2}{2}}dt$.

4.2 Detection probability in the connection state

In a first stage, the partial correlation output Z_p under hypothesis H_1 can be expressed in an identical form to eqn. (2) with M_f^{+1} and M_f^{-1} replaced by M_p^{+1} and M_p^{-1} ($M_p = M_p^{+1} + M_p^{-1}$), respectively. From the above discussion, the PDF of Z_p under H_1, $p_p(z|H_1)$, follows the Gaussian distribution with mean $m_p = 2PM_p/M_f$ and variance $\sigma_p^2 = 8M_p(\sigma_k^2P + \sigma_k^4)/M_f^2$, while the PDF of Z_p under H_0 denoted by $p_p(z|H_0)$ follows the zero mean Gaussian distribution with variance σ_p^2. Then, the PDF of K_2Z_{max} under hypothesis H_1 can be expressed as

$$p_{max}(z|H_1) = \frac{d}{dz}\left[\left\{1 - Q\left(\frac{z - K_2m_p}{\sqrt{2}K_2\sigma_p}\right)\right\}^{N_w}\right] \tag{4}$$

and the PDF of K_2Z_{max} under H_0 is given by

$$p_{max}(z|H_0) = \frac{d}{dz}\left[\left\{1 - Q\left(\frac{z}{\sqrt{2}K_2\sigma_p}\right)\right\}^{N_w-1} \cdot \left\{1 - Q\left(\frac{z + K_2m_p}{\sqrt{2}K_2\sigma_p}\right)\right\}\right] \tag{5}$$

In a second stage, correlating with the remaining $(M_f - M_p)$-bit access code produces the full correlation value of the access code with length M_f, which is expressed in the same form as eqn. (2). Then, the conditional probability of a successful detection is the probability that the full correlation value exceeds K_2Z_{max}, which is given by

$$P_{DS}^i = \int_{-\infty}^{\infty} p_f(x|H_1)\int_{-\infty}^{x} p_{max}(y|H_1)dydx \tag{6}$$

while, when a false detection occurs, the conditional probability of a false detection is given by

$$P_{DF}^i = \int_{-\infty}^{\infty} p_f(x|H_0)\int_{-\infty}^{x} p_{max}(y|H_0)dydx \tag{7}$$

which can be further derived as

$$P_{DS}^i = \int_{-\infty}^{\infty} \frac{1}{\sqrt{2\pi}\zeta_i}e^{-\frac{(x-2\rho_i)^2}{2\zeta_i^2}} \cdot \left\{1 - Q\left(\frac{x - 2\lambda^2\rho_i}{\sqrt{2K_2}\lambda\zeta_i}\right)\right\}^{N_w} dx \tag{8}$$

and

$$P_{DF}^i = \int_{-\infty}^{\infty} \frac{1}{\sqrt{2\pi}\zeta_i}e^{-\frac{x^2}{2\zeta_i^2}}\left\{1 - Q\left(\frac{x + 2\lambda^2\rho_i}{\sqrt{2K_2}\lambda\zeta_i}\right)\right\} \cdot \left\{1 - Q\left(\frac{x}{\sqrt{2K_2}\lambda\zeta_i}\right)\right\}^{N_w-1} dx \tag{9}$$

where $\lambda = \sqrt{K_2M_p/M_f}$.

Finally, the total probabilities of a successful detection and a false detection can be obtained as follows $P_D = (1-r)P_{DS}^1 + rP_{DS}^2$ and $P_{FA} = (1-r)P_{DF}^1 + rP_{DF}^2$, respectively.

5. NUMERICAL RESULTS AND DISCUSSIONS

Numerical behaviors of the proposed synchronization scheme in the Bluetooth network are presented in this section. Throughout this section the parameters $M_f = 64$, $N_w = 20$, and $B = 1$ MHz are assumed. The values of weighting factors K_1 and K_2 are chosen to ensure P_{FA} an acceptable rate for each value of E_b/N_0 and E_b/N_J.

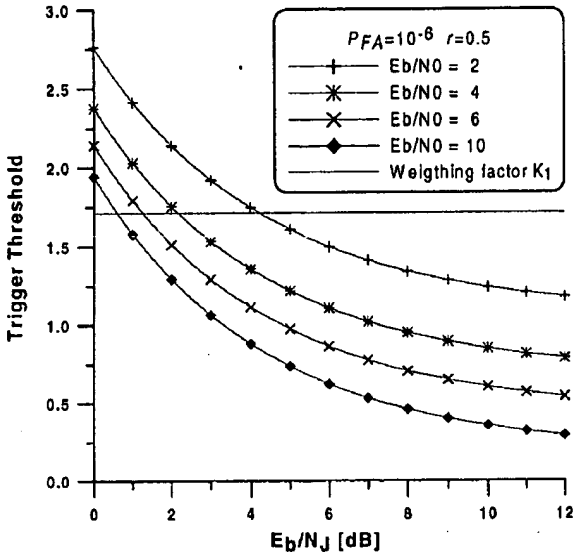

Fig. 7. Trigger threshold versus E_b/N_J for various values of E_b/N_0 ($P_{FA} = 10^{-6}$ and $r = 0.5$)

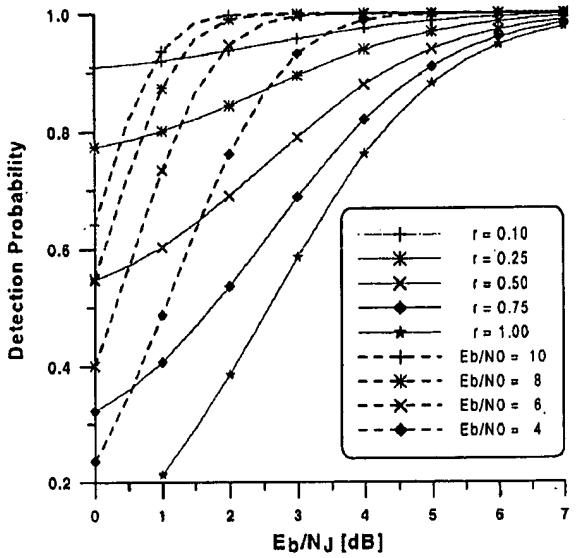

Fig. 8. Performance of the synchronization receiver for various values of r and E_b/N_0 with $P_{FA} = 10^{-6}$: (1) solid line - $E_b/N_0 = 2$ [dB] and (2) dashed line - $r = 1.0$

5.1 Numerical behavior in the initial state

Figs. 7 $\sim$ 8 present the performance of the timing synchronization receiver in the initial state for various system and channel parameters under the partial-band noise environments. Though the master does not broadcast message, the correlation output of slave's unit may exceed the threshold $\sigma_k^2 K_1$ due to the noise interferences during the initial state. Under hypothesis H_0, this happens with probability $P_{FA} = (1-r)Q(K_1/\zeta_1) + rQ(K_1/\zeta_2)$.

Fig. 7 presents the actual trigger threshold versus E_b/N_J with $r = 0.5$ and $P_{FA} = 10^{-6}$. The solid line represents the values of K_1 for various values of E_b/N_0 and E_b/N_J. It is clear from Fig. 7 that values of the weighting factor K_1 is insensitive to the partial-band noise interferences and an adaptive setting of the actual trigger threshold can be obtained by setting the weighting factor to a fixed value.

Performance of the synchronization receiver for various values of partial-band jamming fractions r and E_b/N_0 with $P_{FA} = 10^{-6}$ is shown in Fig. 8. As expected, for lower E_b/N_J, a severe degradation in the detection probability due to the partial-band jamming noise is observed. For a partial-band jamming fraction of $r = 1$, however, the performance degradation according to the variation of E_b/N_0 is negligible, which is thanks to the deemphasis of jammed hops provided by the nonlinear combining scheme. The output of correlation detector when a hop contains a large amount of interference will be smaller than the output when interference is not present, and the hops without interference will have a greater influence on the detection performance.

5.2 Numerical behavior in the connection state

The performance of the timing synchronization receiver in the connection state for various system and channel parameters is examined under the partial-band noise environments in Figs. 9 $\sim$ 12.

Fig. 9 illustrates the sensitivity of the detection probability with respect to the scale factor K_2 and M_p for a fixed value of $E_b/N_0 = E_b/N_J = 6$ [dB] and $r = 0.25$. It is shown in Fig. 9 that the product value of K_2 and M_p to give $P_D > 0.9$ is about less that 50. In the case of Fig. 9, therefore, the synchronization detection can be appropriate as long as the parameters K_2 and M_p are selected to satisfy the condition $K_2 M_p < 50$. Also, a severe degradation in the detection probability due to the improper setting of system parameters can be observed.

Performance of the synchronization receiver for partial-band jamming fractions r with $P_{FA} = 10^{-6}$, $M_p = 30$, and $E_b/N_0 = 6$ [dB] is depicted in Fig. 10. It is observed from Fig. 10 that the variation of the detection probability is insignificant as compared with that of detection probability in Fig. 8. This is due to the fact that the RX timing is based on the latest successful trigger during a master-to-slave slot in the connection state, i.e., the Bluetooth unit has the addresses and clocks of units in range.

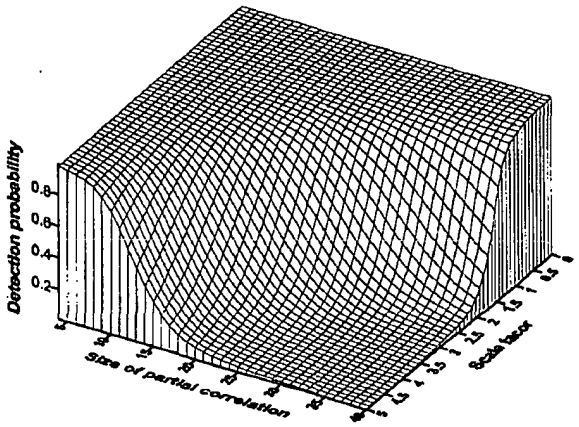

Fig. 9. Sensitivity of the detection probability with respect to various values of K_2 and M_p with $E_b/N_0 = E_b/N_J = 6$ [dB] and $r = 0.25$

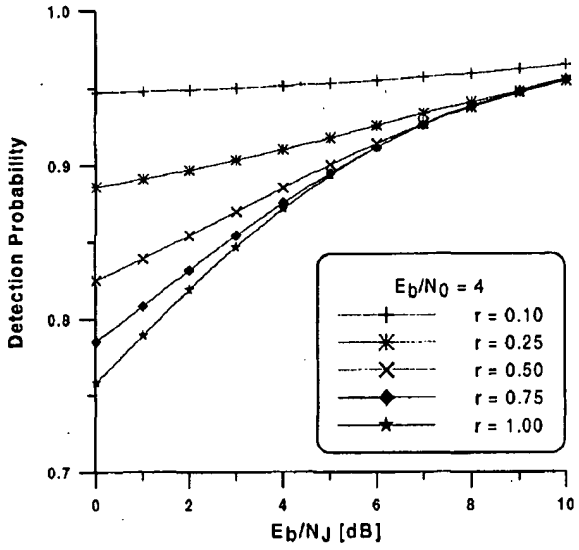

Fig. 10. Performance of the synchronization receiver for partial-band jamming fractions of $r = 0.1$, 0.25, 0.5, 0.75, and 1.0 ($P_{FA} = 10^{-6}$, $M_p = 30$, and $E_b/N_0 = 6$ [dB])

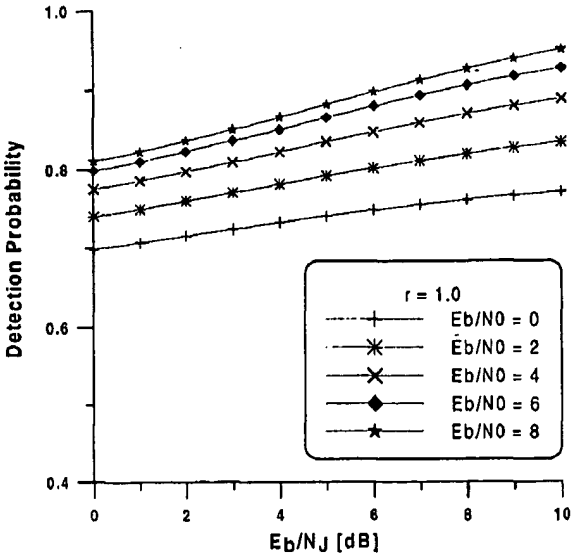

Fig. 11. Performance of the synchronization receiver for various values of E_b/N_0 ($P_{FA} = 10^{-6}$, $M_p = 30$, and $r = 1.0$)

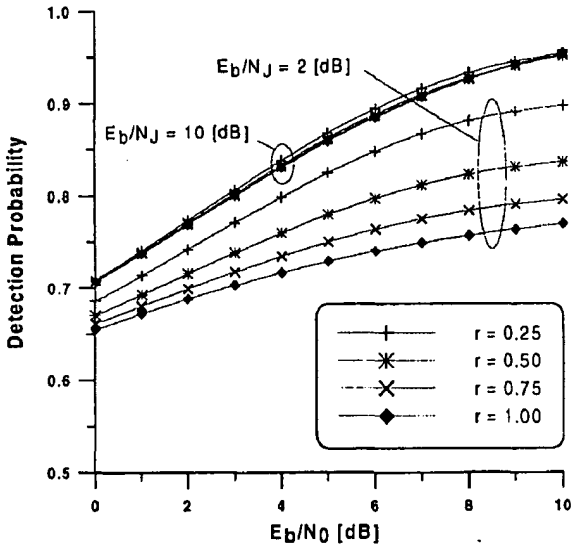

Fig. 12. Performance of the synchronization receiver for partial-band jamming fractions of $r = 0.25$, 0.5, 0.75, and 1.0 with $E_b/N_J = 2$ and 10 [dB] ($P_{FA} = 10^{-6}$ and $M_p = 30$)

Fig. 11 presents the detection performance of the synchronization receiver for various values of E_b/N_0 and E_b/N_J with $P_{FA} = 10^{-6}$, $M_p = 30$, and $r = 1.0$. It is shown from Fig. 11 that the detection probability is less sensitive to the variation of E_b/N_J and the thermal noise is a dominating term compared with the jamming noise.

Fig. 12 shows the influence of the partial-band jamming noise on the detection probability for various values of E_b/N_0 with $P_{FA} = 10^{-6}$ and $M_p = 30$. For higher E_b/N_J, the degradation of the detection performance due to the unwanted partial-band jamming noise is negligible. On the other hand, for lower E_b/N_J, the detection probability of the synchronization receiver depends heavily on the partial-band jamming noise.

6. CONCLUSIONS

The detection performance of the proposed synchronization receivers for a short-ranged radio system has been addressed in the partial-band noise environments. Their synchronization performance is robust against the partial-band noise jamming interferences. Especially, these schemes is suitable for the low-cost and low-complexity technologies like Bluetooth, HomeRF, and HomeCast.

REFERENCES

[1] Bluetooth SIG groups, "Specification of the bluetooth system," ver 1.0 draft foundation, July 1999.
[2] HomeRF, "Technical summary of the SWAP specification," February 1999.
[3] J. S. Lee, R. H. French, and L. E. Miller, "Probability of error analyses of a BFSK frequency-hopping system with diversity under partial-band jamming interference-Part I: Performance of a square-law linear combining soft decision receiver," *IEEE Trans. Commun.*, vol. 32, no. 6, pp. 645-653, June 1984.
[4] L. E. Miller, J. S. Lee, and A. P. Kadrichu, "Probability of error analyses of a BFSK frequency-hopping system with diversity under partial-band jamming interference-Part III: Performance of a square-law self-normalizing soft decision receiver," *IEEE Trans. Commun.*, vol. 34, no. 7, pp. 669-675, July 1986.
[5] F. Bennet *et al.*, "Piconet: embedded mobile networking," *IEEE Personal Commun.*, pp. 8-15, October 1997.
[6] J. G. Proakis, *Digital Communications*, 2nd Ed. New York: MacGraw-Hill, 1989.

Young-Hwan You was born in Pochun, Korea, in 1970. He received the B.S., M.S., and Ph.D. degrees in electronic engineering from Yonsei University, Seoul, Korea, in 1993, 1995, and 1999, respectively.

He is currently a senior researcher at the system IC research center, Korea Electronics Technology Institute (KETI), PyungTaek-Shi, KyungGi-Do, Korea. His research interests are in the areas of wireless/wired communications systems design, spread spectrum transceivers, and system architecture for realizing advanced digital communications systems, especially, for wireless personal area networks (WPAN).

Min-Chul Ju was born in Masan, Korea, in 1974. He received the B.S. degree in Electronic and Electrical Engineering from Pohang University of Science and Technology, Pohang, Korea, in 1997, and the M.S. degree at Korea Advanced Institute of Science and Technology (KAIST), Taejon, Korea, in 1999, respectively.

He is currently a researcher at the system IC research center, Korea Electronics Technology Institute (KETI), PyungTaek-Shi, KyungGi-Do, Korea. His research interests include data communications, spread-spectrum systems, and wireless personal area networks (WPAN).

Jong-Ho Paik was born in Jinhae, Korea, in 1970. He received the B.S and M.S degrees in school of electrical and electronic engineering from ChungAng University, Seoul, Korea, in 1994 and 1997, respectively.

He is currently a researcher at the system IC research center, Korea Electronics Technology Institute (KETI), PyungTaek-Si, KyungGi-Do, Korea. His research interests are in the areas of wireless/wired communications system design, video communications system design and system architecture for realizing advanced digital communications system, especially, for wireless personal area networks (WPAN).

Jin-Woong Cho was born in KyungGi-Do, Korea, on September 1964. He received the B.E. and M.E. degrees from Kwangwoon University, Seoul, Korea, in 1986 and 1988, respectively.

He joined Korea Electronics Technology Institute (KETI) in 1992, where he has been researching and developing wireless communication system. He worked as STA fellow for Electrotechnical Laboratory in Japan in 1999.

Hyoung-Kyu Song was born in CungCheong-Bukdo, Korea on May 14 in 1967. He received B.S., M.S., and Ph.D. degree in electronic engineering in 1990, 1992, and 1996 respectively from Yonsei University, Korea.

From 1996 to 2000 he had been managerial engineer in Korea Electronics Technology Institute (KETI), Korea. Since 2000 he has been an assistant professor of the Department of information and communications engineering, Sejong University, Seoul, Korea. His research interests include digital and data communications, information theory and their applications with an emphasis on mobile communications.